Impacts of Urban Processes and Urbanization on Summer Precipitation: A Case Study of Heavy Rainfall in Beijing on 1 August 2006

SHIGUANG MIAO

Institute of Urban Meteorology, China Meteorological Administration, Beijing, China, and National Center for Atmospheric Research, Boulder, Colorado*

FEI CHEN

National Center for Atmospheric Research, Boulder, Colorado*

QINGCHUN LI AND SHUIYONG FAN

Institute of Urban Meteorology, China Meteorological Administration, Beijing, China

(Manuscript received 17 March 2010, in final form 22 December 2010)

ABSTRACT

Finescale simulations (with 500-m grid spacing) using the Weather Research and Forecasting Model (WRF) were used to investigate impacts of urban processes and urbanization on a localized, summer, heavy rainfall in Beijing. Evaluation using radar and gauge data shows that this configuration of WRF with three-dimensional variational data assimilation of local weather and GPS precipitable water data can simulate this event generally well. Additional WRF simulations were conducted to test the sensitivity of simulation of this storm to different urban processes and urban land-use scenarios. The results confirm that the city does play an important role in determining storm movement and rainfall amount. Comparison of cases with and without the presence of the city of Beijing with respect to the approaching storm shows that the urban effect seems to lead to the breaking of the squall line into convective cells over the urban area. The change of precipitation amount depends on the degree of urbanization (i.e., the change over time in the extent of Beijing city). Model results show that an early urbanization prior to 1980 decreases the maximum rainfall, whereas further urbanization in Beijing is conducive to bifurcating the path of rainfall. According to sensitivity results with a single-layer urban canopy model, the thermal transport (sensible and latent heating) induced by the presence of an urban area apparently is more important than associated momentum transport, with latent and sensible heating apparently having equally important roles in the modification of simulated precipitation. Urban surfaces tend to cause the rainfall to be more locally concentrated. High-rise urban cores may bifurcate the path of rainfall as well as increase the area percentage of heavy rainfall.

1. Introduction

The Greater Beijing metropolitan area in China has experienced a rapid urbanization in the last 30 years, becoming one of the 10 largest megacities in the world, with a population of more than 10 million. Such urban expansion, with increasing built-up areas and human activities, results in significant modifications in the underlying surface properties and atmospheric circulations. Although Zhang et al. (2009) documented a general reduction of summer rainfall as urban area increased in the greater Beijing region, heavy rainfall in the center of the city may be significantly higher (Li et al. 2005), thereby inducing flooding and property losses that result in large economic costs.

Effects of urban processes on precipitation have been widely investigated. Observational and modeling studies show that urban effects lead to increased warm-season precipitation over and downwind of major cities (e.g., Landsberg 1970; Huff and Changnon 1972, 1973; Changnon 1979; Jaurequi and Romales 1996; Shepherd

* The National Center for Atmospheric Research is sponsored by the National Science Foundation.

Corresponding author address: Shiguang Miao, IUM/CMA, 55 Beiwaxili Road, Haidian District, Beijing, 100089, China.
E-mail: sgmiao@ium.cn

DOI: 10.1175/2010JAMC2513.1

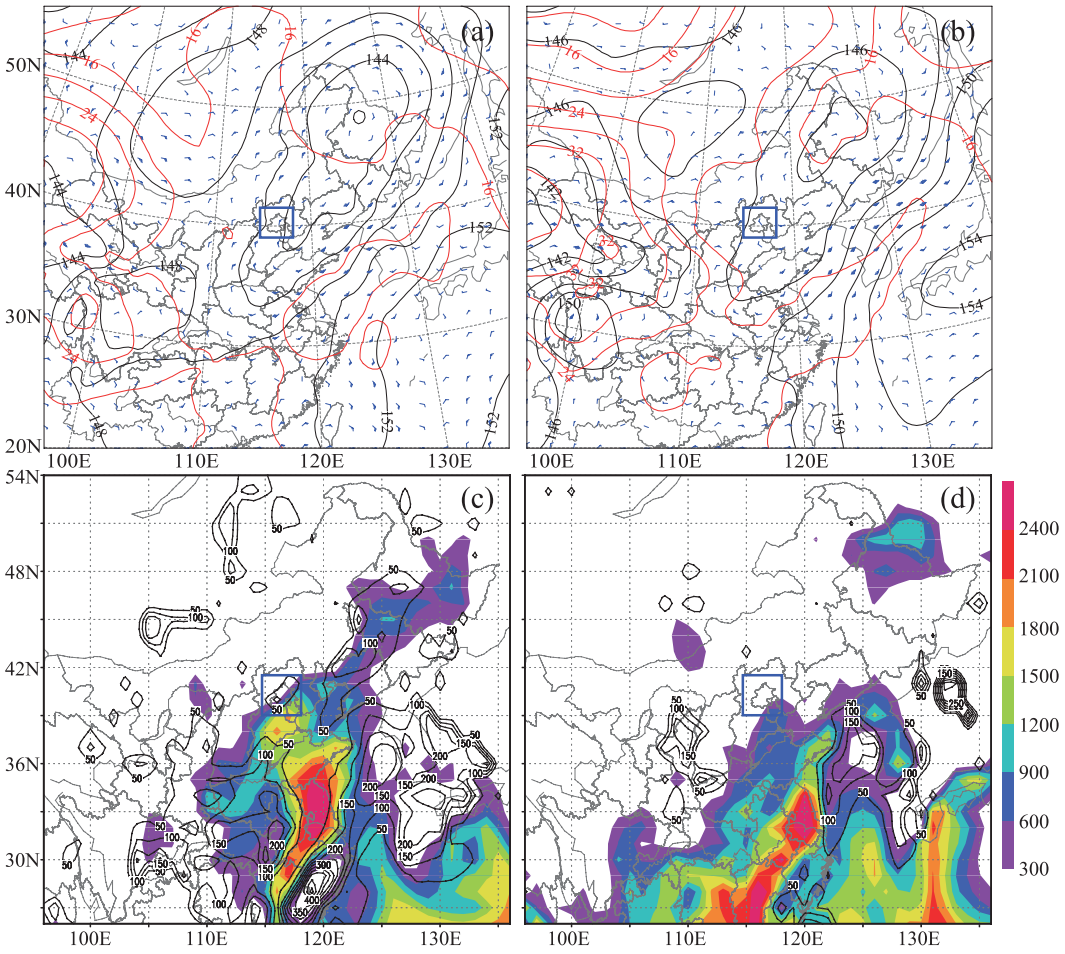

FIG. 1. The synoptic weather pattern at (a) 0000 UTC (0800 LST) and (b) 1200 UTC (2000 LST) 1 Aug 2006 at 850 hPa, showing geopotential height (dam; black lines) and temperature (°C; red lines) with contour intervals of 20 m and 4°C, respectively. The horizontal distributions of CAPE (shaded; J kg^{-1}) and CIN (contours; J kg^{-1}) at (c) 0000 UTC (0800 LST) 31 Jul and (d) 0600 UTC (1400 LST) 1 Aug 2006. The blue rectangles shows the position of Beijing city and the spatial extent of Fig. 3.

et al. 2002). Bornstein and Lin (2000) analyzed data from a surface meteorological network around Atlanta, Georgia, to show that the urban heat island (UHI) induced a convergence zone that initiated storms during the summer of 1996. Many modeling studies have documented that urban areas can enhance surface convergence and rainfall downwind from the city (e.g., Hjemfelt 1982; Craig and Bornstein 2002; Rozoff et al. 2003). On the other hand, precipitation downwind of an urban area may also decrease as a result of urban pollution (Rosenfeld et al. 2007) or as a result of evaporation (Zhang et al. 2009).

For Beijing, Guo et al. (2006) and Zhang et al. (2009) studied the presence of urban land cover on modeling convective precipitation events. Their results suggested that, after urbanization, decreases in surface latent heat flux induced by the presence of urban areas led to reduction of convective available potential energy (CAPE) and hence to weaker summer precipitation. Given these seemly contradicting results, one question to be posed is: Are the impacts of cities on rainfall different at different stages of urbanization?

Significant progress in modeling urban surface fluxes [reviewed by Masson (2006) and Souch and Grimmond (2006)] provides an excellent opportunity to address this question. In general, there are three approaches to account for urban effects in mesoscale meteorological models. These are 1) the bulk roughness approach (e.g., Liu et al. 2006), 2) single-layer urban canopy models (UCM) (e.g., Masson 2000; Kusaka et al. 2001), and 3) multilayer UCMs (e.g., Martilli et al. 2002; Dupont et al. 2004). The single-layer UCM (SLUCM; Kusaka et al. 2001) has been coupled to the ''Noah'' land surface model (LSM) (Chen and Dudhia 2001) in the community

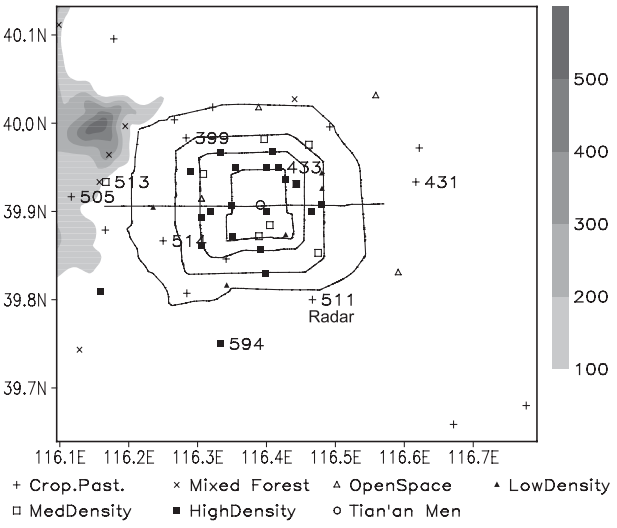

FIG. 2. The distribution of surface observation stations over different land uses (represented by various symbols). Terrain height is shown with shading (m). The black contours delineate, from inner to outer, the second, third, fourth, and fifth circles; the transverse line is Chang'an Street; and the open circle represents the position of Tian'an Men.

mesoscale Weather Research and Forecasting (WRF) Model, version 2.2, (Kusaka et al. 2001; Chen et al. 2006, 2011). This SLUCM is in the middle of the spectrum of urban modeling methods within mesoscale models, and it is a compromise between urban model complexity and computational resources required to execute urban models. It takes urban building geometry and the associated radiative, thermal, and moisture effects into account in its surface energy budget and wind shear calculations. The coupled WRF–SLUCM has been evaluated against surface and boundary layer observations (Lin et al. 2008; Miao et al. 2009a; Wang et al. 2009). This coupled mesoscale atmospheric–urban modeling system enables us to study further the mechanism of urban effects on the rainfall.

More recent papers allude to a complexity of aerosol effects. Urban areas produce large amounts of pollution that increase the number of cloud condensation nuclei (CCN) in the atmosphere. This decreases the mean droplet radius, creating a lack of coalescence, and inhibits precipitation formation (Rosenfeld et al. 2007). A modeling study by van den Heever and Cotton (2007)

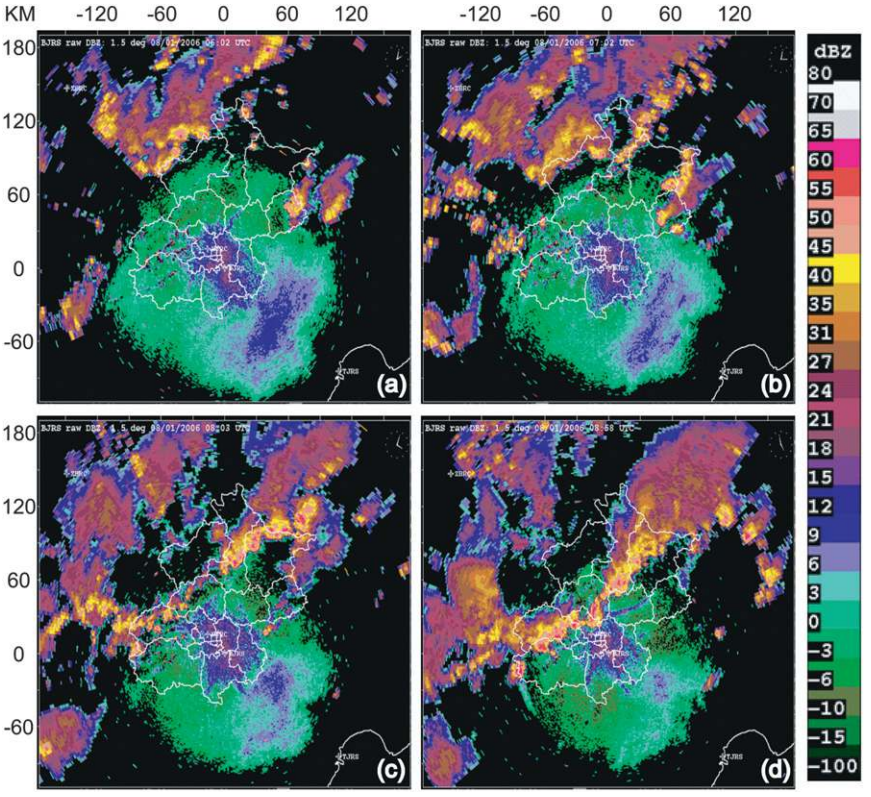

FIG. 3. The reflectivity observed by Beijing S-band radar: (a) 0602 UTC (1402 LST), (b) 0702 UTC (1502 LST), (c) 0803 UTC (1603 LST), and (d) 0858 UTC (1658 LST) 1 Aug 2006. The white lines represent Beijing's district borders.

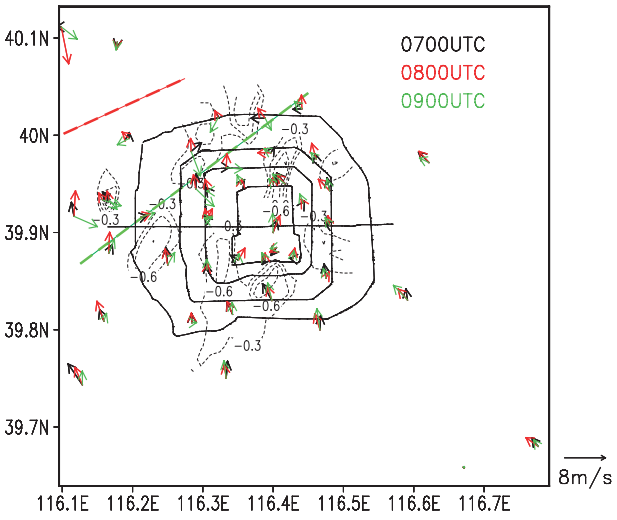

FIG. 4. The observed wind fields at 10 m AGL at 0700 UTC (1500 LST; black), 0800 UTC (1600 LST; red), and 0900 UTC (1700 LST; green) 1 Aug 2006. The dashed contours show the horizontal divergence every 0.3 $(1000\ s)^{-1}$ calculated from the observation on 0700 UTC (1500 LST). The dashed lines are the estimated positions of wind shear.

suggested that giant CCN in an urban environment may offset the microphysical suppression role of smaller CCN. By warming air aloft, high concentrations of aerosols can cool the surface, decrease CAPE, and suppress convective clouds. When microphysical effects are more dominant than these radiative effects, there could be an invigoration of convection (Rosenfeld et al. 2008), with stronger updrafts producing higher cloud heights that lead to increased precipitation amounts and events (van den Heever and Cotton 2007).

In this paper, finescale simulations (with 500-m grid spacing) conducted with the WRF–SLUCM were used to investigate impacts of urban processes and expansion on a localized summer heavy rainfall event in Beijing. While recognizing the importance of urban aerosol in rainfall formation as indicated by Rosenfeld et al. (2008), we focus on the thermodynamic and dynamic influences of the city on precipitation. Our main objective is to assess the impact of simulated treatments of various urban processes on the initiation and movement of a heavy summer precipitation event and the degree of urbanization

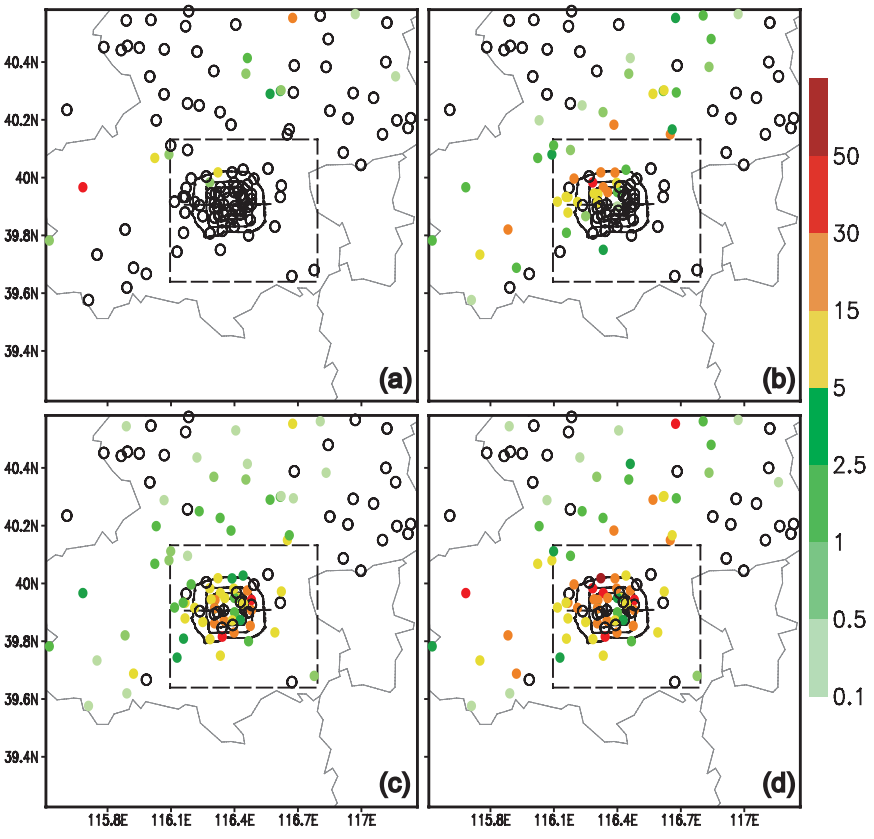

FIG. 5. The observed hourly rainfall (mm) at (a) 0900 UTC (1700 LST), (b) 1000 UTC (1800 LST), and (c) 1100 UTC (1900 LST) and 3-h accumulated rainfall (mm) for (d) 0800–1100 UTC (1600–1900 LST) 1 Aug 2006. The dashed rectangle shows the fifth domain D05 (with 500-m grid spacing) for WRF numerical simulations. Solid lines, other than those in D05, represent province borders.

to which the modeled precipitation is sensitive. For this, WRF is used to conduct a number of sensitivity tests that include different degrees of complexity in representing urban processes and urban land-use scenarios. In section 2, the observed rainfall characteristics are analyzed. In section 3 we describe the WRF–Noah–SLUCM numerical simulations. The validations of the control case are presented in section 4, and we close with discussions of sensitivity tests (section 5), followed by a summary and discussion in section 6. Note that the results presented in this study may be limited by the use of a single-layer UCM, by the selected case (only one 24-h simulation), and by the absence of aerosol–cloud interactions.

2. Case selected: Observed rainfall characteristics

A selected summer case is investigated in this study because it allows us to discern urban effects for local convective heavy rainfall. Between 0000 UTC (0800 LST) and 1200 UTC (2000 LST) 1 August 2006, an already weak low pressure system moved over the Beijing area at 500, 700, and 850 hPa and weakened slightly more (only the weather patterns from observation at 850 hPa are shown in Figs. 1a and 1b). So the synoptic pattern is almost steady in this period. Figures 1c and 1d [using the final (FNL) operational global analysis data on 1° × 1° grids by the National Centers for Environmental Prediction (NCEP)] show that, in comparison with the regional large CAPE and a little convective inhibition (CIN) around Beijing city on 0000 UTC (0800 LST) 31 July 2006, the CAPE and CIN over Beijing City on 0600 UTC (1400 LST) 1 August 2006 are very small. Zhao and Wang (2008) analyzed and compared the synoptic patterns of two successive torrential rain events that occurred in Beijing on 31 July and 1 August 2006 using observation and NCEP analysis data. Their Fig. 4 (not shown here) revealed that the long-distance transport of moisture from south to north and the colliding of cold air and warm air over the Beijing area on 1 August 2006 became weaker relative to those on 31 July 2006. This synoptic pattern is not conducive to form regional rainfall but is favorable to initiate local rainfall. This scenario is ideal to study the more localized impacts of how urban land uses initiate and modify local rainfall.

As seen in Fig. 2, 60 surface observation stations (equipped with the automatic weather station MAWS301 by Vaisala, Inc.) are located over different land-use types, and an S-band radar is located at station 511 south of downtown Beijing. The typical spacing of the stations in the urban area of Fig. 2 is ~5 km, and 17 stations are considered urban.

At 0602 UTC (1402 LST) 1 August 2006 (see Fig. 3), some convective cells started to form at high elevations

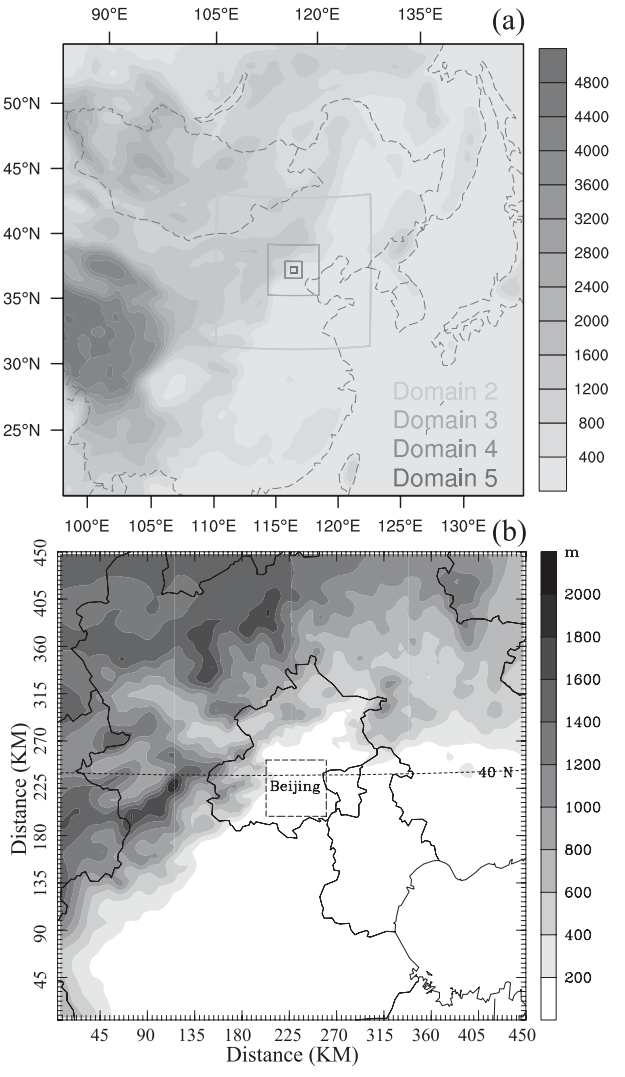

FIG. 6. Configuration of (a) the five two-way nested domains and (b) D04 and D05 for the WRF–Noah–UCM simulation. Shading is terrain height in meters.

west of Beijing and moved southeasterly and intensified into a squall line across downtown Beijing. The temporal variation of surface wind when the squall line approached the downtown is shown in Fig. 4. At 0700 UTC (1500 LST), there are southerly and southeasterly flows while the convective cells are formed west of downtown (Fig. 3b). Convergence zones in the urban area are evident, are correlated with the building height distribution shown in Fig. 7a, and most likely are induced by urban circulations (or UHI circulations). At 0800 UTC (1600 LST), the squall line is formed (Fig. 3c) and the wind shear maximum (red dashed line in Fig. 4) shifts to the north of downtown. One hour later, the squall line is developed and approaching (Fig. 3d) and the wind shear penetrates into the downtown with strong confluence.

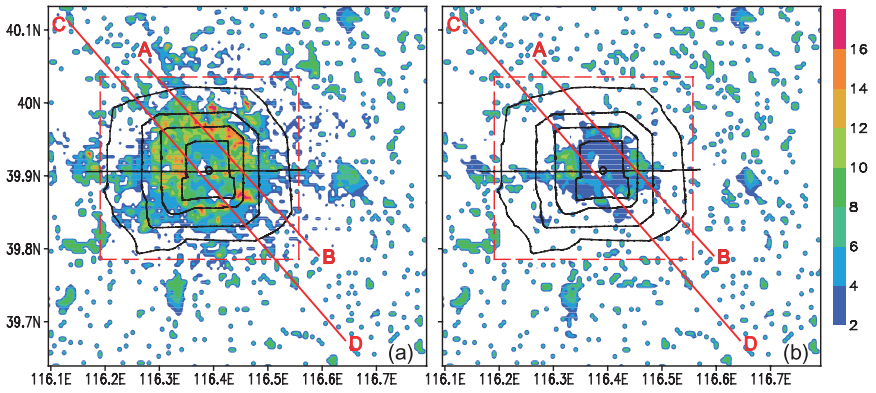

FIG. 7. The distribution of building height (m) in the fifth domain with 500-m grid spacing for cases (a) CTRL and (b) U80. The red dashed rectangle shows the extent of "full urban" in case FU. Red lines AB and CD indicate the positions of cross sections shown in Figs. 14 and 16.

Simultaneous with these events, it begins to rain downtown (Fig. 5). Figure 5c shows two heavy-rainfall centers at 1100 UTC (1900 LST) in the highly developed downtown area with higher buildings (shown in Fig. 7a), presumably associated with urban effects. The 3-h rainfall accumulation (Fig. 5d; a zoom over the downtown region is shown in Fig. 12a) pattern shows three rainfall centers in the high-density urban area, each with more than 30 mm of total rainfall observed. The maximum 1-h (3-h) rainfall in Beijing reaches 32.4 mm (55 mm) at the upwind edge (northwestern part) of downtown.

3. WRF–Noah–SLUCM numerical simulations

Many operational forecast centers are moving toward higher-resolution models for short-range weather forecasting applications. One motivation for this is to provide improved forecasts of hazardous weather and, in particular, severe convection. First, the increased resolution is expected to enable the model to represent mesoscale features that would otherwise not be resolved and to represent convection explicitly rather than by a convection parameterization. Second, higher-resolution models are able to make use of high-resolution input data.

Lean et al. (2008) investigated the characteristics of high-resolution versions of the Met Office Unified Model for forecasting convection over the United Kingdom and concluded that, although there are problems involving too-small convective cells in some situations, the 1-km model generally performs better than the 4-km model with regard to convective initiation and the general scales evident in the precipitation fields. Based on the fifth-generation Pennsylvania State University–National Center for Atmospheric Research (NCAR) Mesoscale Model (MM5), Liu et al. (2006) developed a real-time, multigrid (grid increments of 0.5–45 km), four-dimensional data-assimilation (RTFDDA) and forecasting system (Cram et al. 2001) that has been in operational use at five U.S. Army test ranges since 2001.

TABLE 1. The characteristics of sensitivity tests described in the text (for details, see text).

		Physical processes in urban area simulated by UCM			
Expt	Land-use map	Dynamics	Sensible heat flux	Latent heat flux (humidity)	The max of 3-h accumulated rainfall (mm)
CTRL	Current		All		55.5
Different physical processes in urban area simulated by UCM					
NOUCM	Current		No		26.1
DYN	Current	Yes	No	No	16.5
NODYN	Current	No	Yes	Yes	47.6
NOHUM	Current	Yes	Yes	No	34.0
Different land-use maps					
U2C	No urban		All		26.5
U80	1980s		All		19.3
FU	Full urban		All		51.6

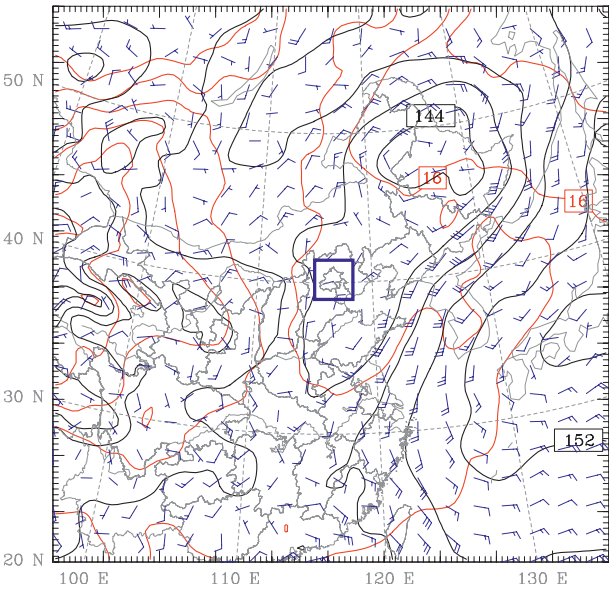

FIG. 8. As in Fig. 1, but for WRF results at 1200 UTC (2000 LST) 1 Aug 2006 at 850 hPa (9-h forecast of D1).

The WRF is a next-generation community numerical weather prediction system designed to serve both operational forecasting and atmospheric research needs. It is suitable for a broad spectrum of applications across scales ranging from meters to thousands of kilometers (Skamarock et al. 2005). The coupled WRF–Noah–SLUCM with 500-m horizontal grid spacing can simulate the characteristics of the UHI and boundary layer structures generally well (Miao et al. 2009a). In this study, it is used to investigate the mechanism of urban effects on the rainfall. Further, LeMone et al. (2010) performed a number of idealized runs with grid spacing of 0.2, 0.333, 0.5, and up to 10 km, and the simulated convective structures appear to be anomalous only when using a grid spacing of 333 m. Note that their study used the Yonsei University PBL scheme (YSU) and simulated fair-weather convection. For idealized tropical cyclones, Rotunno et al. (2009) used 500 m and YSU, and the deep convection was well simulated. When they used only large-eddy simulation (LES) with 67-m resolution, however, there was not enough turbulence, and they even needed to turn on the PBL scheme in addition to LES. At 500-m resolution, use of the Mellor–Yamada–Janjic (MYJ) scheme and YSU produced similar and reasonable results.

We integrate the Advanced Research WRF (ARW, version 2.2) described by Skamarock et al. (2005) over five nested domains (Fig. 6). Note that the SLUCM in the latest WRF (version 3.2) is the same as that used here. The horizontal grid spacings (numbers of grid cells) of these five domains are 40.5 km (100 × 100), 13.5 km (100 × 100), 4.5 km (100 × 100), 1.5 km (100 × 100), and 0.5 km (118 × 109), respectively. The vertical grid contains 38 full sigma levels from the surface to 50 hPa, of which the lowest 13 levels are below 1 km to have finer resolution in the PBL.

To take urban geometry into account in its surface energy budgets and wind shear calculations, this WRF–Noah–SLUCM coupled modeling system (Chen et al. 2006, 2011) includes 1) 2D street canyons parameterized to represent the effects of urban geometry on urban canyon heat distribution; 2) shadowing from buildings and reflection of radiation in the canopy layer; 3) canyon orientation and a diurnal cycle of solar azimuth angle; 4) streets consisting of eight canyons with different orientations; 5) Inoue's model for canopy flows; 6) a multilayer heat equation for roof, wall, and road interior temperatures; and 7) a very thin bucket model for evaporation and runoff from road surfaces. It was further enhanced to include the calculation of wind speed within the urban canopy and the incorporation of anthropogenic heat associated with energy consumption by human activities. This model was evaluated over the Beijing metropolitan area (Miao and Chen 2008; Miao et al. 2009a). The lowest model level is 0.994 (i.e., the half level is at ~30 m) to meet the requirement of SLUCM. The wind speed in the urban canopy is calculated using the building frontal area index instead of a drag coefficient (Coceal and Belcher 2005). The hourly anthropogenic heating is estimated from 2006 statistical energy

TABLE 2. Comparison of the simulated (control case) and observed variables from 0300 to 0800 UTC (1100–1600 LST) 1 Aug 2006 before the first rainfall hour (N_stn: number of stations, Mean: mean value, Std dev: standard deviation, RMSE: root-mean-square error, IOA: index of agreement, HR: hit rate, Obs: Observation, V_Tr: traditional variables, and V_UC: variables in the urban canopy). The criteria for hit-rate calculation for 2-m temperature, 10-m wind speed, and 2-m specific humidity are 2°C, 1 m s^{-1}, and 2 g kg^{-1}, respectively.

		Mean			Std dev			Mean bias		RMSE		IOA		HR	
Variable	N_stn	Obs	V_Tr	V_UC	Obs	V_Tr	V_UC	V_Tr	V_UC	V_Tr	V_UC	V_Tr	V_UC	V_Tr	V_UC
2-m temperature	43	32.79	32.85	33.16	0.68	0.49	0.58	0.07	0.17	0.94	0.81	0.60	0.69	0.95	0.98
10-m wind speed	42	1.56	1.71	0.62	0.62	0.79	0.27	0.15	−0.82	1.08	1.02	0.51	0.46	0.64	0.63
2-m specific humidity	30	12.84	11.76	11.82	0.96	0.50	0.44	−1.08	−1.00	1.60	1.51	0.40	0.41	0.75	0.77

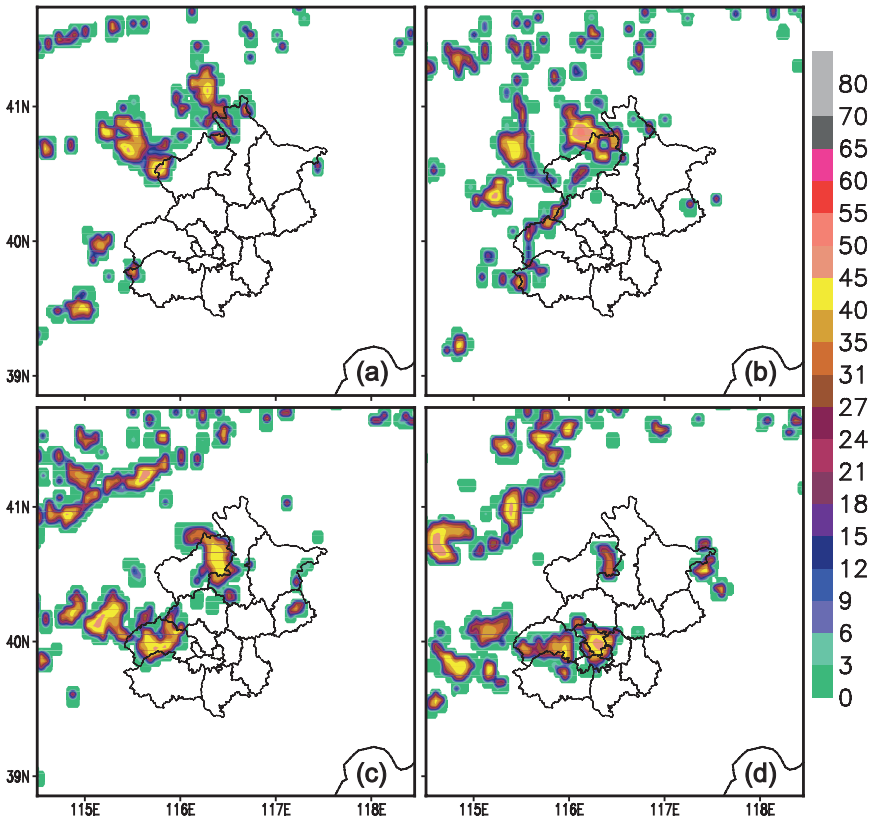

FIG. 9. As in Fig. 3, but for model results.

consumption and traffic data obtained from Beijing Municipal Bureau of Statistics (2006) and used by Miao et al. (2009a).

Fan et al. (2008) showed that the assimilation of local GPS precipitable water data improved the performance of a quantitative rainfall forecast of the high-resolution WRF (27/9/3 km) in the Beijing area. To get better initial and boundary conditions for the numerical simulation of this rainfall event, the WRF three-dimensional variational data assimilation (3D-Var) system was used on five domains for the initial time to incorporate local automatic weather station and ground-based GPS precipitable water data in the Beijing area. The first-guess atmospheric fields are from the NCEP FNL operational global analyses on a 1.0° × 1.0° grid, and the initial soil conditions are obtained from the U.S. Air Force Weather Agency's agricultural meteorology modeling system (AGRMET) data. The precipitable water data are from 29 ground-based GPS stations distributed in the Beijing, Huairou, and Fangshan areas with horizontal resolution of ~10 km. The half-hourly signals GPS stations received are transformed to precipitable water information by the Bernese software package. The soil state for the LSM is just an interpolation from global data from AGRMET, which is an offline land data assimilation system using the Noah LSM (Chen et al. 2007), so that WRF and AGRMET have the same climatological soil states. AGRMET has been running continuously since 2004; therefore the soil states used in this study have been spun up reasonably. A plot of initial skew T (not shown) indicates that the initial field is sufficient to capture the differences between rural and urban areas that are found in and above the boundary layer. A 24-h simulation (0300 UTC 1 August 2006–0300 UTC 2 August 2006) was conducted to assess the model's performance.

We use the MYJ PBL scheme (Janjic 1990, 1994), which predicts turbulent kinetic energy and allows vertical mixing between individual layers within the PBL. The urban roughness lengths were increased to affect the momentum. Other physical parameterizations include the WRF Single-Moment 6-Class Microphysics Scheme (WSM6), the shortwave radiation scheme (Dudhia 1989), the Rapid Radiative Transfer Model longwave radiation scheme, and the Noah LSM (Chen and Dudhia 2001; Ek et al. 2003). The Grell–Devenyi ensemble cumulus scheme (Grell and Devenyi 2002) is used for the 40.5- and 13.5-km domains; there is no subgrid convective parameterization applied to the finer domains. The SLUCM,

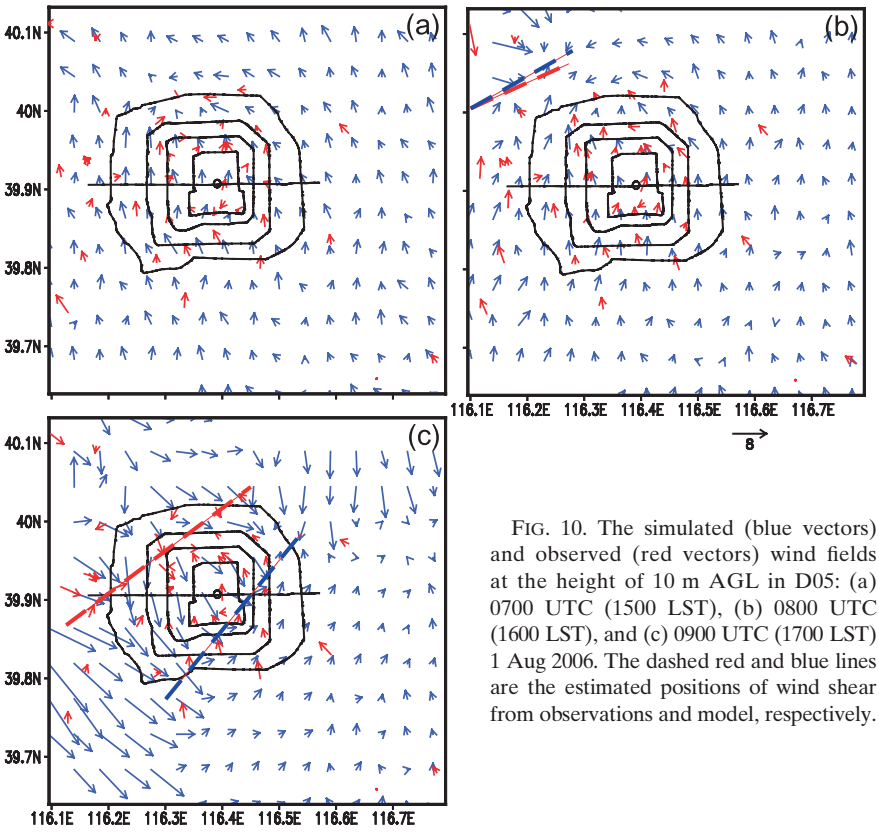

FIG. 10. The simulated (blue vectors) and observed (red vectors) wind fields at the height of 10 m AGL in D05: (a) 0700 UTC (1500 LST), (b) 0800 UTC (1600 LST), and (c) 0900 UTC (1700 LST) 1 Aug 2006. The dashed red and blue lines are the estimated positions of wind shear from observations and model, respectively.

suitable for a grid spacing from 1 km to several kilometers, is used for the 4.5-, 1.5-, and 0.5-km domains. Two-dimensional urban fraction data are used in the numerical simulation to combine the fluxes from SLUCM and the Noah LSM.

a. Control case

For the control case (referred to as CTRL), land-use/land-cover data with horizontal resolution of 500 m, building morphology, and statistical energy consumption data for Beijing were used to derive two-dimensional urban parameters for the UCM (Miao et al. 2009a,b). Figure 7a depicts the distribution of the building heights for the WRF fifth domain with a grid spacing of 500 m. Tall and dense buildings with relatively narrow roads are located between the second circle and the fifth circle, resulting in a small sky view factor (SVF) and a large amount of anthropogenic heating. The SVF is used in the calculation of shortwave and longwave radiation in the SLUCM. A small SVF will capture more radiation. Anthropogenic heat is added to the surface energy budget equation. Large amounts of anthropogenic heat will cause high air temperature and strong UHI.

b. Sensitivity cases

WRF was also used to test the sensitivity of the simulation of this storm to the treatment of various urban processes (e.g., dynamic and thermodynamic effects) and to different urban land-use scenarios (e.g., no urban, urbanization prior to 1980, and further urbanization). The characteristics of these sensitivity tests are summarized in Table 1.

Retaining the same land-use distribution and urban parameters as in CTRL, four tests were performed to investigate the impacts of different physical processes in urban area on the boundary layer structure and rainfall:

1) the NOUCM case, which has no UCM but uses the default Noah LSM with simple urban treatment (the bulk roughness approach),
2) the DYN case, which uses the UCM but with only the dynamic effect of urban (there is no sensible heat and latent heat from urban; rather those from the Noah LSM over a cropland/grassland mosaic are used),
3) the NODYN case, which uses the UCM but excludes the dynamic effects of the UCM (the momentum flux from the Noah LSM over a cropland/grassland mosaic is used), and

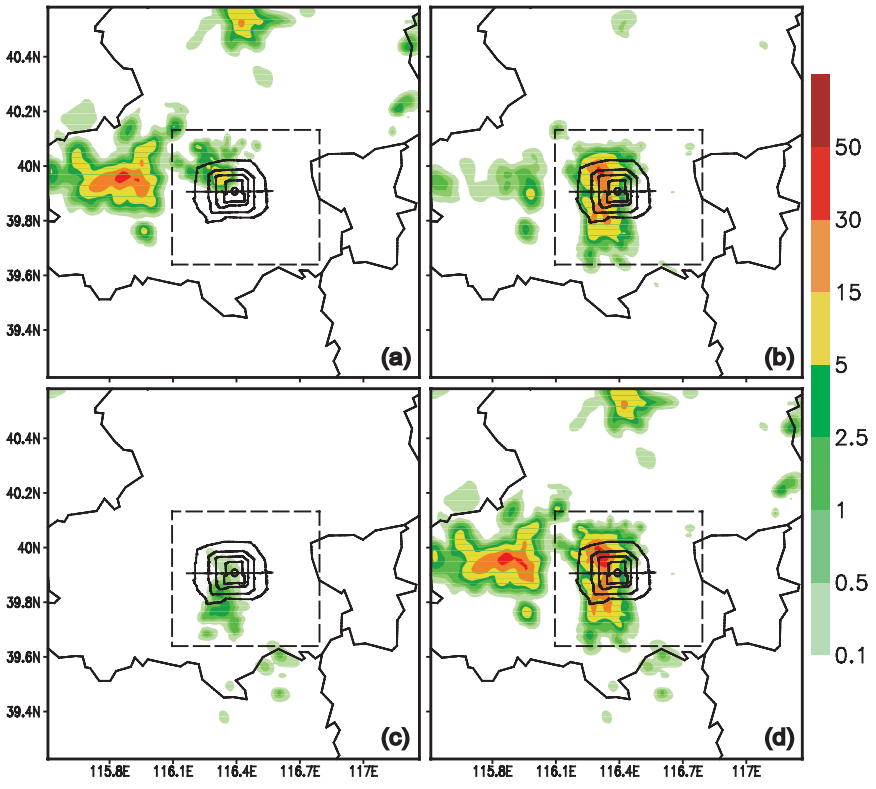

FIG. 11. As in Fig. 5, but for model results.

4) the NOHUM case, which uses the UCM but excludes the humidity effects of the UCM (there is no latent heat from urban; rather that from Noah LSM over a cropland/grassland mosaic is used).

Three additional cases are conducted for different land-cover and land-use maps and corresponding urban parameters:

1) the U2C case, in which all urban land-use grid points in domain 5 in the control case are replaced by dry cropland (USGS category 2), which is the background land-use type in rural areas surrounding Beijing city,
2) the U80 case, which replaces the land-cover map in the fifth domain with that of 1980s and in which the parameters for UCM are also changed to those of the 1980s according to high-resolution land-use, land-cover, building-morphology, and statistical energy-consumption data for the 1980s (the distribution of building heights in the 1980s is shown in Fig. 7b, which is different from Fig. 7a and reflects the fact that the urban area in the 1980s was very small and the mean building height was very low), and
3) the FU case, in which, to represent a further urbanization scenario, all grid points in the domain within the dashed rectangle of Fig. 7 except the water body and the grids with mean building heights of higher than 10 m are converted into high-density urban land use (using the default urban parameters in the table of WRF–Noah–SLUCM with mean building height of 10 m).

All of these sensitivity experiments are conducted using initial/boundary conditions and physics schemes that are identical to those in the CTRL simulation.

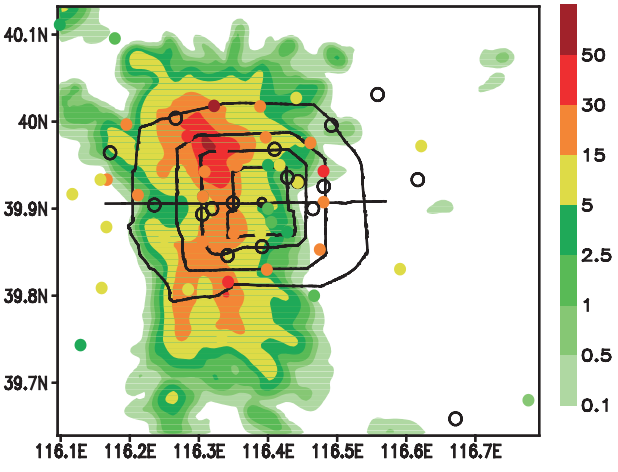

FIG. 12. The observed (shaded circles) and simulated (shaded) 3-h accumulated rainfall (mm) for 0800–1100 UTC (1600–1900 LST) 1 Aug 2006.

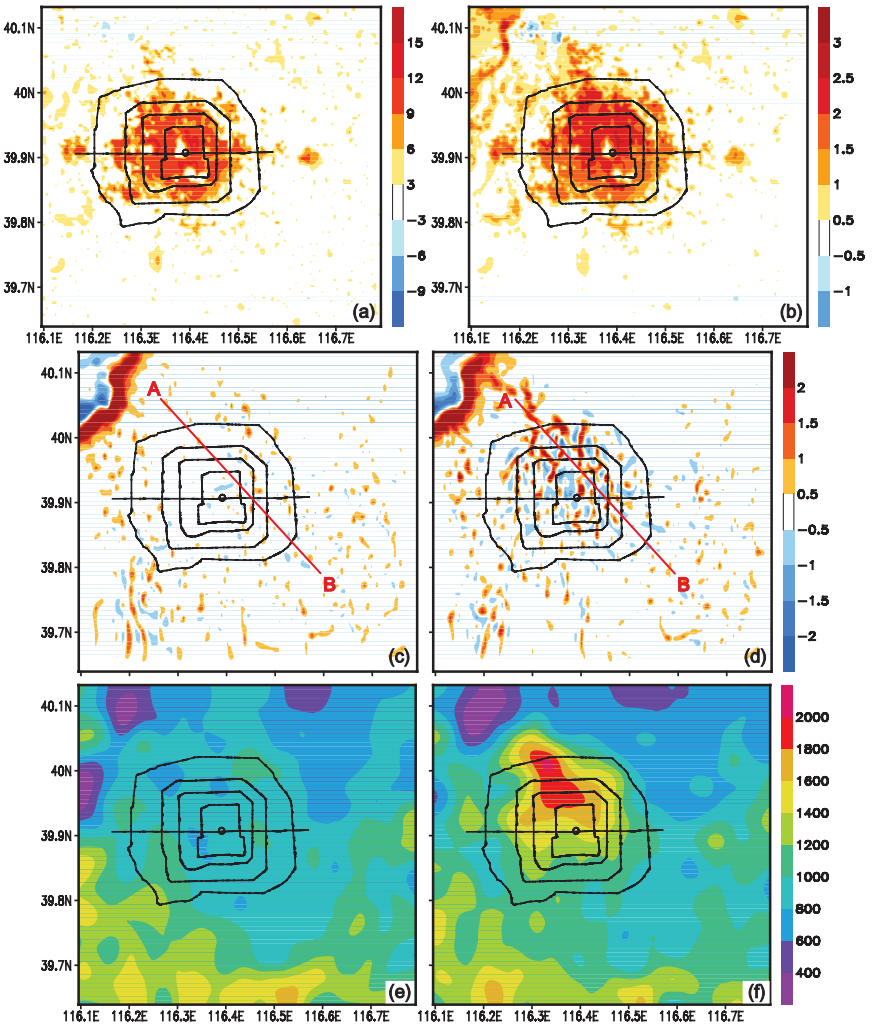

FIG. 13. Horizontal distribution of WRF results at 0800 UTC (1600 LST) 1 Aug 2006: the difference fields of (a) land surface temperature and (b) 2-m air temperature between case CTRL and case U2C, the vertical velocity of cases (c) U2C and (d) CTRL; and spatially filtered PBL height (see text for details) of cases (e) U2C and (f) CTRL. Red line AB indicates the position of the cross section shown in Fig. 14.

4. Validation of control case

The WRF accurately simulated the general synoptic weather pattern and in particular the geopotential height pattern and temperature distribution at 1200 UTC (2000 LST, the ninth forecast hour) 1 August 2006 at 850 hPa, although the fields in the Tibetan plateau do show some departures (Fig. 8), which are partly due to the impacts from the domain boundary.

The verification statistics of 2-m temperature, 10-m wind speed, and 2-m specific humidity from the 0.5-km domain from 0300 to 0800 UTC (1100–1600 LST) 1 August 2006 before the first rainfall hour include the index of agreement (IOA; Pielke and Pearce 1994), hit rate (HR; Schlünzen and Katzfey 2003), and other statistics (Table 2). The observations from the automatic weather stations are used for comparison. The HR, a categorical measure and a comparison with a threshold value, is a reliable overall measure for describing model performance because it is able to consider the measurement uncertainty, which is difficult to consider in the bias or the root-mean-square error (RMSE). The criteria for HR calculation are for model–observation agreement within 2°C for 2-m temperatures, 1 m s^{-1} for wind speed, and 2 g kg^{-1} for 2-m specific humidity, following the forecast accuracy desired in Cox et al. (1998).

The mean bias (MB) of simulated 2-m temperature is very small (0.07°C), RMSE is less than 1°C (0.94°C), and HR is very high (0.95). The urban canopy temperatures from WRF–Noah–SLUCM averaged over 25 urban

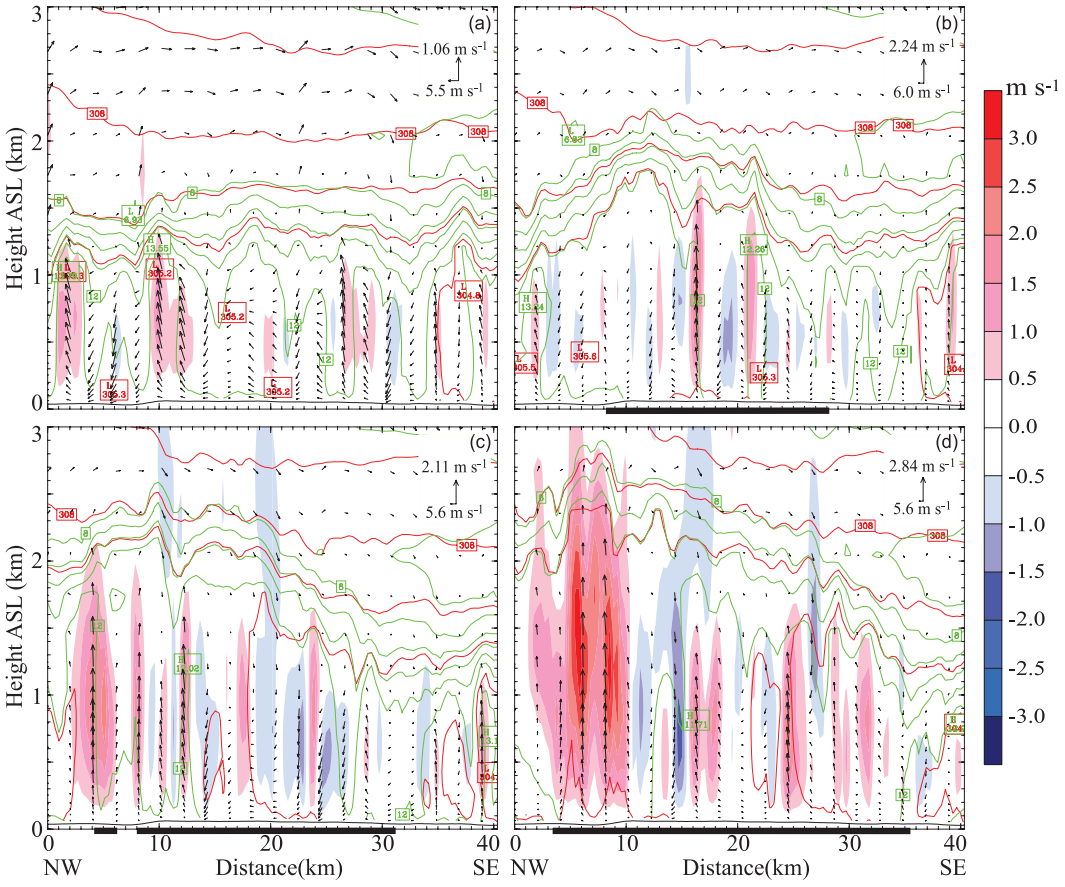

FIG. 14. Cross section of vertical velocity (shaded; m s^{-1}), potential temperature (red contour at every 1 K), water vapor mixing ratio (green contour at every 1 g kg^{-1}), and circulation vectors (m s^{-1}; reference vector at top-right of each panel) along line AB (shown in Figs. 7 and 13c,d) at 0800 UTC (1600 LST) 1 Aug 2006 for cases (a) U2C, (b) U80, (c) CTRL, and (d) FU. Vector scales at the top-right corner of every panel indicate the maximum. The urban area is marked with a solid black horizontal line.

stations (33.16°C) are 0.31°C higher than the corresponding 2-m temperature averaged for all of 43 stations (32.85°C). The mean 10-m wind speed from the model is slightly larger than that from the observations, and its RMSE is around 1 m s^{-1}. The modeled urban-canopy wind speed averaged over 25 urban stations (0.62 m s^{-1}) is 1.09 m s^{-1} lower than 10-m wind speed averaged over all of 42 stations (1.71 m s^{-1}). The model is drier than the observation, and IOA for 2-m humidity is the smallest among these three variables, partly because of the lack of anthropogenic moisture sources in the WRF–Noah–SLUCM. The anthropogenic moisture is mainly from air conditioning in buildings, irrigation, street cleaning, and vehicle emissions. Most attempts to quantify anthropogenic emissions have focused on the sensible heat component, largely ignoring moisture emissions (Sailor 2011). The low IOA values for temperature are partly due to the short data series (5 h). Note that the urban-canopy variables (V_UC in Table 2, the outputs from SLUCM) are approximately at one-half of the mean building height, ranging from 0.5 to 10 m.

The weighted HRs of this period, calculated by weighting the single HRs of three variables (2-m temperature, 10-m wind speed, and 2-m specific humidity) by the number of comparison data, are 0.78 and 0.80 for conventional variables and urban-canopy variables, respectively, which are higher than those from the simulation of a clear day with the same model configuration (0.65 and 0.73) (Miao et al. 2009a). Sensitivity simulation shows that the three-dimensional data assimilation used in this case is largely responsible for this improvement.

In summary, these error statistics are within acceptable ranges, suggesting that the WRF–Noah–SLUCM system simulates the meteorological fields before the rainfall event generally well.

The plots of skew T (not shown) indicate that the model captures the evolvement of the boundary layer over the first hours. Comparison of modeled reflectivity

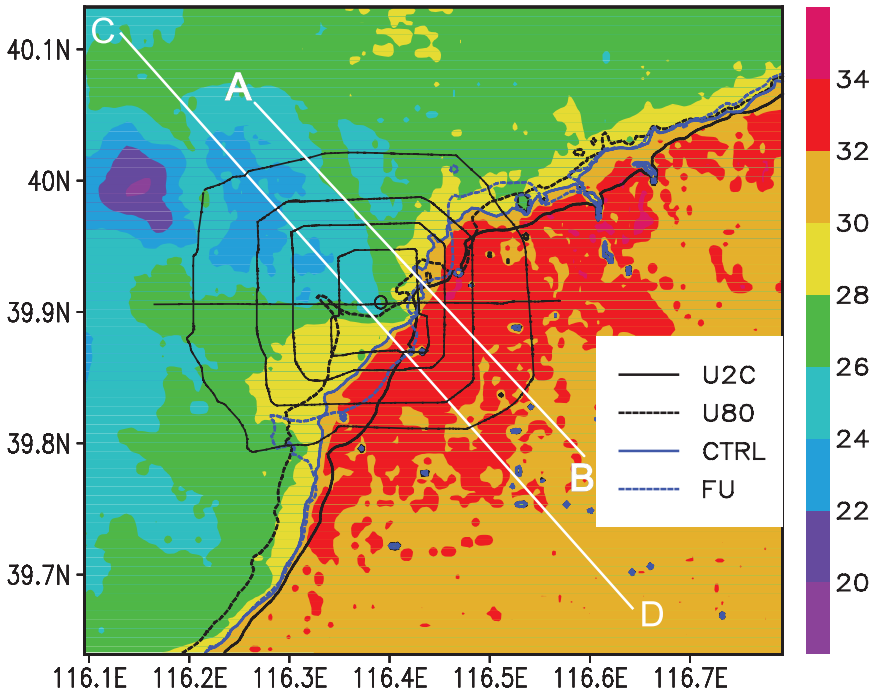

FIG. 15. Horizontal distribution of 2-m temperature for case CTRL at 0900 UTC (1700 LST) 1 Aug 2006. Four solid and dashed lines indicate the position of 30°C isotherm for the four cases. White lines AB and CD indicate the positions of the cross sections shown in Fig. 14 and Figs. 16 and 17, respectively.

(Fig. 9) with observations (Fig. 3) at the onset of precipitation in the fifth domain shows that the model simulates the initiation, development, and movements of this event fairly well, especially for the location and timing of the convection. Nevertheless, some cells in the northwest of Beijing are missed, and subsequently the upper-right part of the squall line is not well simulated. This can be expected given the nature of these highly localized convections. The mislocated part of the convection is a little far from the urban area, and therefore this may not affect the sensitivities of the model results much.

The simulated surface wind fields in Fig. 10 show southerly wind at 0700 UTC (1500 LST), which agrees well with the observation (red vectors). At 0800 UTC (1600 LST) when the storm approaches the downtown area, the position of wind shear (surface convergence line) from the model (dashed blue line) is consistent with that from observations (dashed red line). One hour later, the modeled convergence line penetrates into the downtown area farther than the observed one does (i.e., the storm movement from the model is faster).

The sensitivity test without urban land use (case U2C, discussed later) shows that the faster movement is not due to the urban canopy modeling. Rather, it is sensitive to the treatment of microphysics in WRF. Our sensitivity tests with different microphysics schemes indicated that (not shown) 1) using the Kessler scheme produces a smaller maximum of 3-h accumulated rainfall (24 mm) than is observed (55 mm) but that the simulated movement of the surface convergence line is generally consistent with the observations, 2) using the Lin scheme produces larger rainfall (78 mm) and quicker movement, and 3) using the Ferrier scheme or the Thompson scheme produces smaller rainfall (20 and 16 mm, respectively) and slower movement. By contrast, the WSM6 scheme used in the CTRL case produces rainfall (55 mm) that is similar to that observed. When compared with the observed 12 mm of the maximum of hourly rainfall from 0800 to 0900 UTC (1600–1700 LST), the simulated heavier rainfall (20 mm) results in stronger downdrafts, which are presumed to be responsible for the faster movement in CTRL case. Therefore the microphysics scheme has tangible impact on the development of the storm. The model captures the wind distribution and temporal variation generally well, however.

The simulated rainfall in the fourth domain (Fig. 11) agrees reasonably well with the observation of the general movement of the system producing the rainfall (Fig. 5). As seen in the surface wind fields, however, the simulated rainfall is earlier than the observed rainfall. For the 3-h rainfall in the fifth domain (Fig. 12), the simulated

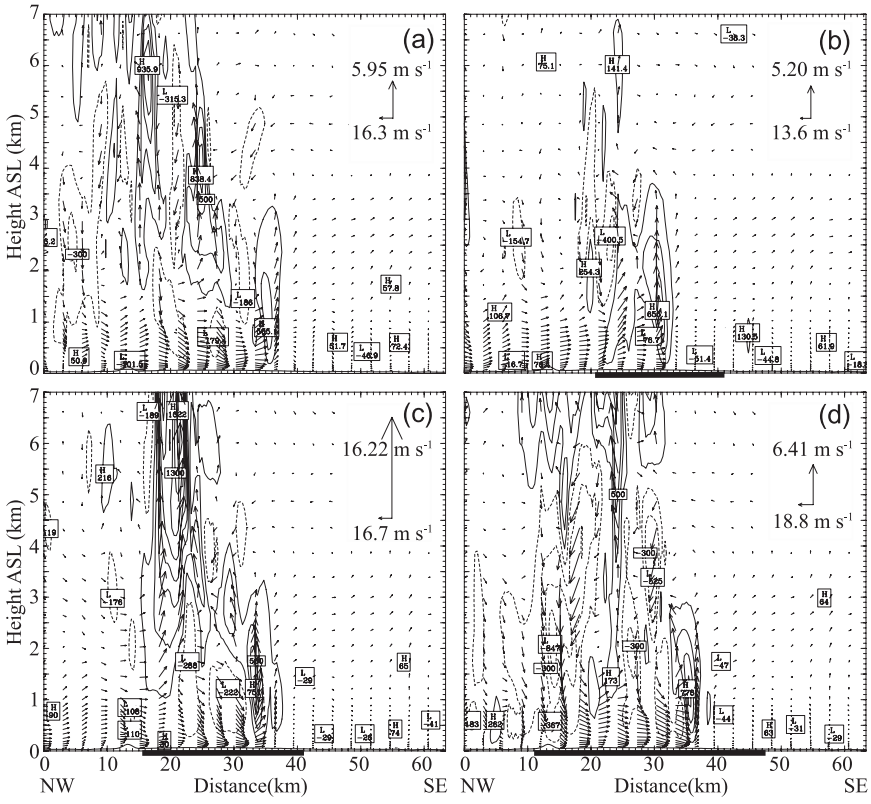

FIG. 16. Cross sections of vertical velocity (contours; cm s^{-1}) and circulation (vectors) along line CD in Fig. 15 at 0900 UTC (1700 LST) 1 Aug 2006 for cases (a) U2C, (b) U80, (c) CTRL, and (d) FU. Vector scales at the top-right corner of each panel indicate the maximum. The urban area is marked with a solid black horizontal line.

maximum rainfall reaches 55.5 mm in the northwestern part the city (between the second circle and the fifth circle), despite missing a small rainfall center in the eastern part of the city and a small area of rainfall in the western part of the city. Overall, model performance under these configurations is adequate to examine different permutations of starting conditions.

5. Numerical simulations of urban processes and urbanization effects on precipitation

Comparison between CTRL and U2C (Fig. 13) shows that at 0800 UTC (1600 LST, the fifth forecast hour) 1 August 2006 urban areas substantially increase the land surface temperature (>15°C) and 2-m air temperature (>3°C) through urban canopy processes such as shortwave radiation trapping and extra anthropogenic heating, and so on. The vertical mixing in the urban area is stronger, and the PBL is raised to ~1800 m in contrast with ~800 m in nonurban cases. Note that the scale-selective filter used by Barnes et al. (1996) is applied to the PBL height field (shown in Figs. 13e,f) in postprocessing at each grid point with $D = 4$ km selected to eliminate small-scale fluctuations. Cross-sectional fields along line AB (Fig. 14) show that, for U2C, the PBL is wet, homogeneous, and capped by an inversion layer. For U80, the PBL is lifted by stronger vertical mixing and is drier than that in U2C. In the CTRL, the capped inversion layer is eroded in the upwind part of the urban area, which is conducive to the development of convection. For FU, vertical mixing is stronger and the PBL is raised higher, but it is drier than in CTRL.

The 30°C isotherm for the four cases at 0900 UTC (1700 LST) indicates the location of the storm front (Fig. 15). Ahead of the front the 2-m temperature in the urban area is distinctly higher than that in the rural area, whereas behind the front the temperature is reduced because of the rainfall. Among the four cases, the storm movement is fastest for U2C, is slowest for U80, and is similar for CTRL and FU. It suggests that for U80 the drag effect is essential for the slowing down while the storm enhancement due to thermodynamic effect is negligible. For CTRL and for FU, the thermodynamic effect induced by the presence of urban land use

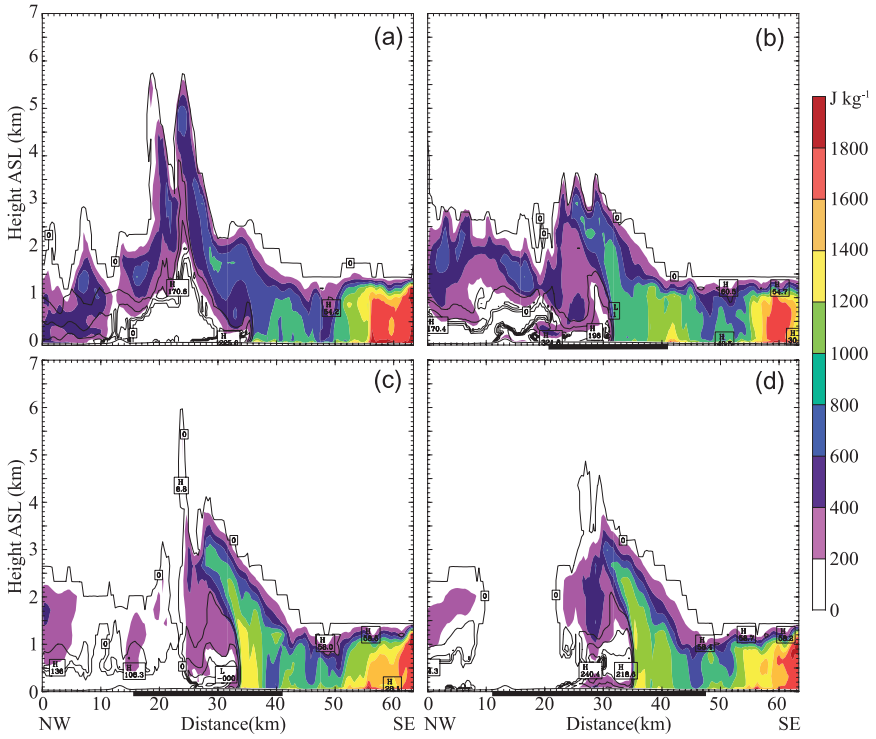

FIG. 17. Cross sections of CAPE (shaded; J kg^{-1}) and CIN (contour; J kg^{-1}) along line CD in Fig. 15 at 0900 UTC (1700 LST) 1 Aug 2006 for cases (a) U2C, (b) U80, (c) CTRL, and (d) FU. The urban area is marked with a solid black horizontal line.

enhances the storm (Figs. 16–21) so that its movement is faster than that for U80. Several studies also showed that urban land cover will affect the storm movement through its building barrier effect (e.g., Bornstein and LeRoy 1990; Bornstein and Lin 2000; Guo et al. 2006).

Cross-sectional fields along line CD (Figs. 16 and 17) show that, when compared with U2C, at 0900 UTC (1700 LST) the updrafts for U80 are weaker, for CTRL they are largely stronger, and for FU they are a little stronger. CAPE is increased ahead of the front with increases in urban density. As compared with the maximum of CIN for case U2C (225.6 J kg^{-1}), CIN for U80 is largely increased to 321.8 J kg^{-1}, whereas for CTRL it is markedly decreased to 136 J kg^{-1}, and for FU it is similar (240.4 J kg^{-1}). These changes will result in changes of maximum and accumulated rainfall (Fig. 21). Furthermore, the storm front for FU is slightly ahead of that for U2C, which implies that the effect on storm movement due to urban thermal enhancement may exceed that due to building barriers. Further analyses (Fig. 18) indicate that, as a result of the penetration of the cold and wet air mass into the downtown area, the difference of sensible heat flux between case FU and case U2C at 0900 UTC (1700 LST) increases markedly when compared with that at 0800 UTC (1600 LST) and that of the latent heat flux increases to about zero. Hence the difference of the sum of sensible and latent heat flux between case FU and case U2C increases dramatically corresponding to urban morphology. The urban drag effect is about 1 m s^{-1} except for the strong downdrafts from the enhanced storm in case FU. Therefore the enhancement and the faster speed of the FU simulation relative to U2C are attributed to increased thermal forcing, which may exceed that due to the building blocking.

For urbanized cases the cells in the urban area (i.e., the fifth domain, denoted by the dashed rectangle in Fig. 19) are separated from the squall line, in contrast to the integrated convections for the nonurban case (U2C) (Fig. 19). This case study suggests that the urban effect leads to the breaking of the squall line to a convective cell over urban areas.

The 3-h accumulated rainfall from 0800 to 1100 UTC (1600–1900 LST) 1 August 2006 for all cases is shown in Fig. 20. The major difference in rainfall between NOUCM (Fig. 20b) and CTRL (Fig. 20a) suggests that properly modeling the complex processes in urban areas with the aid of UCM is necessary for reproducing features of rainfall, especially the amount (26.1 mm as compared

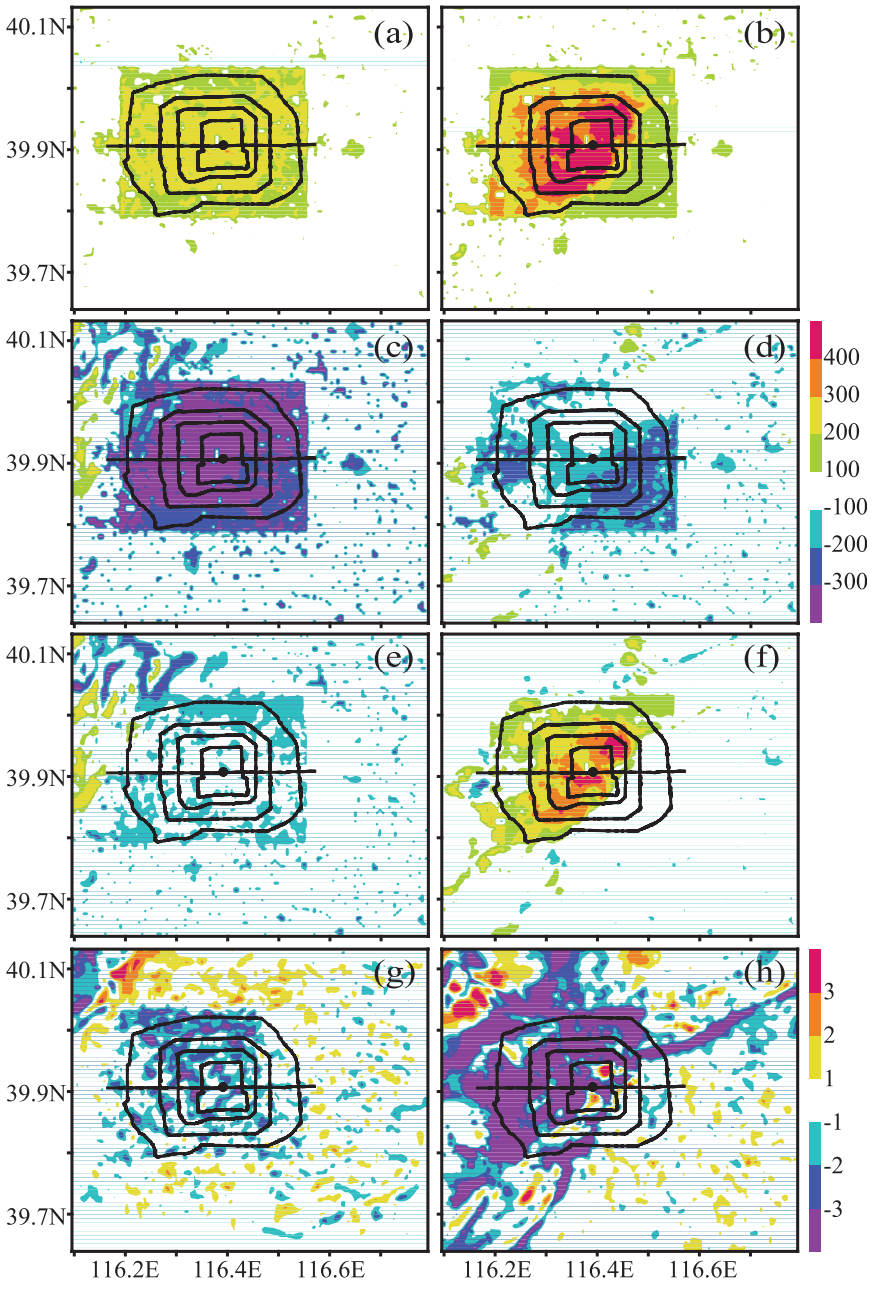

FIG. 18. The difference fields of the simulated (a),(b) sensible heat flux, (c),(d) latent heat flux, (e),(f) sum of sensible and latent heat flux (W m^{-2}), and (g),(h) 10-m wind speed (m s^{-1}) between case FU and case U2C at (left) 0800 UTC (1600 LST) and (right) 0900 UTC (1700 LST) 1 Aug 2006.

with 55.5 mm). Results from sensitivity cases show that the city does play an important role in determining storm movement and rainfall. Without urban areas (U2C in Fig. 20c), rainfall would not move through the city core and reach the southern part of the city; the rain area is dispersed, and its amount is much reduced (26.5 mm as compared with 55.5 mm). Among urban influences, the thermal transport (sensible and latent heating; Fig. 20f) leads to centralized rainfall and appears to be more influential than the momentum transport (Fig. 20d). The thermal transport, latent heating (cf. Figs. 20a,e), and sensible heating (cf. Figs. 20d,e) from urban areas apparently affect simulated precipitation equally. When compared with U2C, however, early urbanization prior

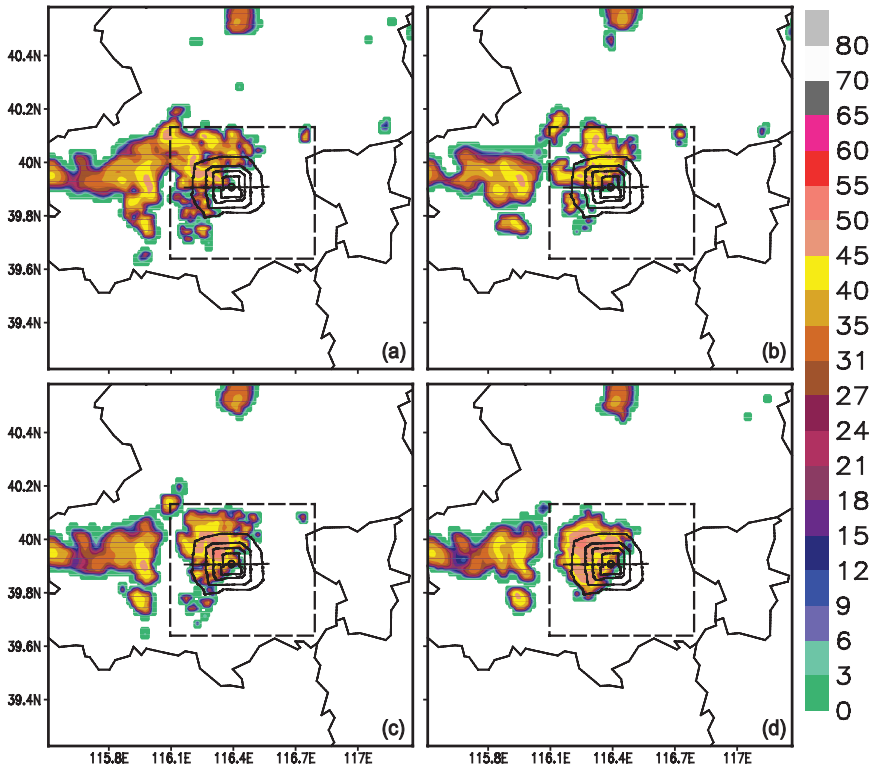

FIG. 19. Horizontal distribution of WRF simulated maximum reflectivity in D04 at 0900 UTC (1700 LST) 1 Aug 2006 for cases (a) U2C, (b) U80, (c) CTRL, and (d) FU.

to 1980 decreases the maximum rainfall (Fig. 20g) but concentrates rainfall distribution. Increasing the urban representation in Beijing split the squall line and slightly decreased the maximum precipitation in this case in comparison with CTRL (Fig. 20h).

The statistics of four cases for different land-use scenarios were expressed as a percentage of the values at 0800–1100 UTC for U2C, the least urbanized case (Fig. 21). The rainfall area increases markedly at 1100 UTC; it is slightly reduced for the whole rain period, however. The accumulated volumetric precipitation increases for CTRL and FU during this event relative to U80. In summary, increasing urban area produces similar areal coverage, but intensity (medium to heavy rainfall, not shown) and total precipitation are nearly 2 times that in the nonurban case.

The percentage of the grid cells with different rainfall intensities over the whole rainfall grids in the fifth domain (not shown) suggests that for the first 2 h of the rainfall period and for the whole period the percentages of heavier rainfall are higher for FU and CTRL than for U2C and U80. For the later rain period (1100 UTC), U80 and CTRL have heavier rainfall. In summary, the general trend is for increasingly heavier rainfall as urban land cover increases.

6. Summary and discussion

This case study of localized heavy rainfall over Beijing, China, was chosen to investigate urban effects on precipitation at a finescale. The type of rainfall event simulated in this study occurs frequently in this area and is a representative weather pattern during summer (Li et al. 2005; Zhao and Wang 2008). Finescale simulations (with 500-m grid spacing) using the WRF–Noah–SLUCM system indicated that the WRF simulates the meteorological fields before the rainfall event generally well. Evaluation using radar, surface wind, and gauge data confirmed that WRF can simulate this event accurately despite missing a small rainfall center at the eastern part of the city. Nevertheless, the simulated storm movement is faster than that observed, presumably because of improper modeling of the convection processes (e.g., the microphysics scheme).

Model results indicate that including the bulk thermal and dynamic effects of the urban canyons as represented in the UCM leads to a reproduction of urban convective rainfall amounts and distribution. Results from sensitivity tests reveal that the representation of the city in the model plays an important role in determining storm movement and rainfall. Urban land cover apparently

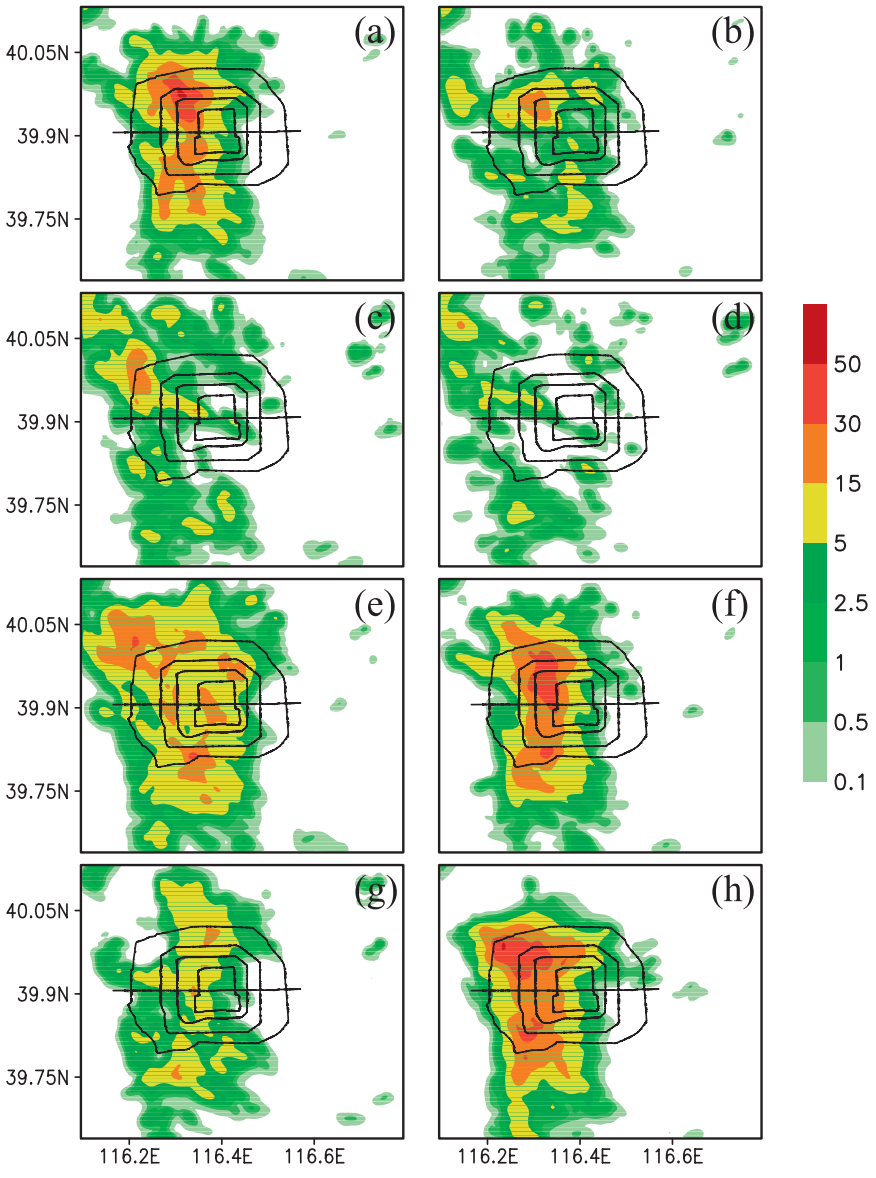

FIG. 20. The 0800–1100 UTC (1600–1900 LST) 1 Aug 2006 3-h accumulated rainfall (mm) from WRF simulations: (a) control case (CTRL), (b) no UCM (NOUCM), (c) no urban (U2C), (d) urban dynamic effect only (DYN), (e) no urban humid effect (NOHUM), (f) no urban dynamic effect (NODYN), (g) urbanization prior to 1980 (U80), and (h) further urbanization (FU).

leads to the breaking of the squall line to a convective cell over urban areas. Moreover, the amount, timing, and location of the precipitation depend on the degree of urbanization. In the early stage of urbanization (e.g., prior to 1980), the main effect is surface drying with weak confluence and uplift associated with the UHI, which reduced maximum rainfall. When the degree of urbanization is increased in WRF (e.g., current and further urbanization), the simulations show stronger UHI effects and vertical mixing, raising the PBL height and weakening the capped inversion intensity, which is conducive to the development of convection and may result in the increase of maximum and accumulated volumetric rainfall.

Furthermore, sensitivities toward various aspects of the UCM were also conducted. Among urban influences, the thermal transport (sensible and latent heating) is apparently more important than the momentum transport for the localized convective rainfall event. Among the thermal transport, latent heating and sensible heating are both very important. In addition, urban land uses tend to cause rainfall to be locally concentrated and to

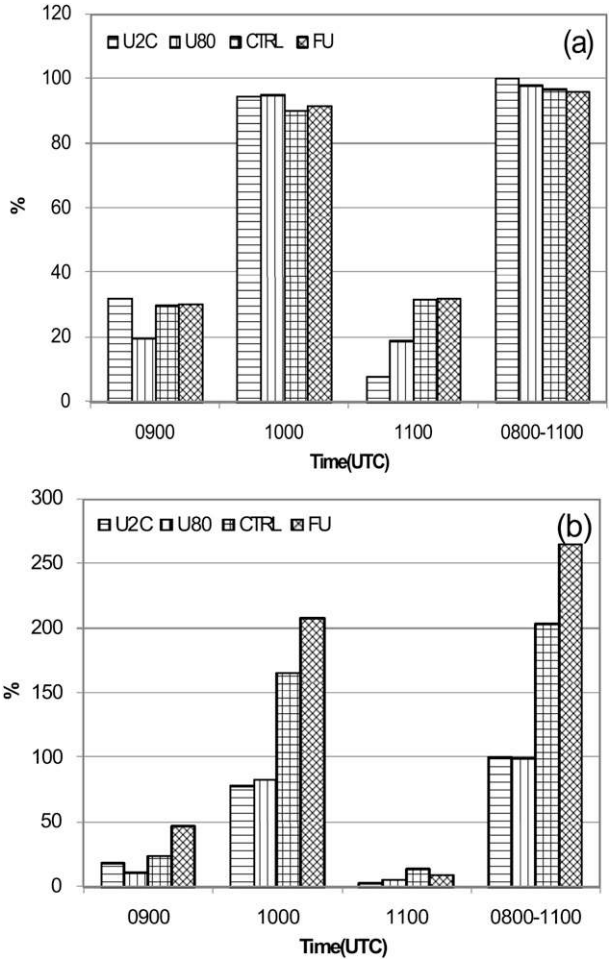

FIG. 21. Time series of (a) the rainfall area [>0.01 in. (0.025 cm)], and (b) the accumulated volumetric precipitation in the fifth domain expressed as a percentage of the values at 0800–1100 UTC for U2C.

bifurcate around high-rise urban cores. Urban land uses may increase the area percentage of heavy rainfall.

Although the WRF–Noah–SLUCM system exhibits suitable performance and reveals some preliminary results about the role of urban processes and urbanization in the rainfall event, caution should be used when interpreting these results because they may be limited by the use of a single-layer UCM and a one-day case study and by ignoring aerosol–cloud interactions. Further testing should be performed on the effects of a sophisticated multilayer UCM (Martilli et al. 2002) with an indoor–outdoor exchange model into the WRF (Chen et al. 2011) on precipitation over and downstream of cities. Further investigations are worth conducting using advanced meteorological–chemical models [for understanding the role of aerosols as suggested by Rosenfeld et al. (2008)], ensemble sensitivity tests, and fine-resolution seasonal simulations including large-scale climatic feedbacks to understand better the complicated and highly nonlinear interactions among regional climate change, synoptic conditions, and land-use patterns.

Acknowledgments. The authors are grateful to three anonymous reviewers for their thoughtful review and valuable comments, which led to improvements in this manuscript. This work was funded by National Natural Science Foundation of China (40505002 and 40775015), the Ministry of Science and Technology of China (2008BAC37B04, 2006BAJ02A01, and GYHY200906026), the Special Foundation for National Commonweal Institutes of China (IUMKY200901), the NCAR FY07 Director Opportunity Fund, and the U.S. DTRA coastal-urban project.

REFERENCES

Barnes, S. L., F. Caracena, and A. Marroquin, 1996: Extracting synoptic-scale diagnostic information from mesoscale models: The Eta Model, gravity waves, and quasigeostrophic diagnostics. *Bull. Amer. Meteor. Soc.,* **77,** 519–528.

Beijing Municipal Bureau of Statistics, 2006: *Beijing Statistical Yearbook 2006.* China Statistics Press, 462 pp.

Bornstein, R., and G. M. LeRoy, 1990: Urban barrier effects on convective and frontal thunderstorms. Preprints, *Fourth Conf. on Mesoscale Processes,* Boulder, CO, Amer. Meteor. Soc., 120–121.

——, and Q. Lin, 2000: Urban heat islands and summertime convective thunderstorms in Atlanta: Three case studies. *Atmos. Environ.,* **34,** 507–516.

Changnon, S. A., Jr., 1979: Rainfall changes in summer caused by St. Louis. *Science,* **205,** 402–404.

Chen, F., and J. Dudhia, 2001: Coupling an advance land surface–hydrology model with the Penn State–NCAR MM5 modeling system. Part I: Model implementation and sensitivity. *Mon. Wea. Rev.,* **129,** 569–585.

——, M. Tewari, H. Kusaka, and T. T. Warner, 2006: Current status of urban modeling in the community Weather Research and Forecast (WRF) Model. *Extended Abstracts, Sixth Symp. on the Urban Environment,* Atlanta, GA, Amer. Meteor. Soc., J1.4. [Available online at http://ams.confex.com/ams/Annual2006/techprogram/paper_98678.htm.]

——, and Coauthors, 2007: Description and evaluation of the characteristics of the NCAR high-resolution land data assimilation system. *J. Appl. Meteor. Climatol.,* **46,** 694–713.

——, and Coauthors, 2011: The integrated WRF/urban modeling system: Development, evaluation, and applications to urban environmental problems. *Int. J. Climatol.,* **31,** 273–288.

Coceal, O., and S. E. Belcher, 2005: Mean winds through an inhomogeneous urban canopy. *Bound.-Layer Meteor.,* **115,** 47–68.

Cox, R., B. L. Bauer, and T. Smith, 1998: Mesoscale model intercomparison. *Bull. Amer. Meteor. Soc.,* **79,** 265–283.

Craig, K. J., and R. D. Bornstein, 2002: MM5 simulation of urban induced convective precipitation over Atlanta. Preprints, *Fourth Symp. on the Urban Environment,* Norfolk, VA, Amer. Meteor. Soc., 5–6.

Cram, J. M., Y. Liu, S. Low-Nam, R.-S. Sheu, L. Carson, C. A. Davis, T. T. Warner, and J. F. Bowers, 2001: An operational mesoscale RT-FDDA analysis and forecasting system. Preprints, *18th Conf. on Weather Analysis and Forecasting and 14th Conf.*

on Numerical Weather Prediction, Ft. Lauderdale, FL, Amer. Meteor. Soc., J2.11. [Available online at http://ams.confex.com/ams/pdfpapers/22389.pdf.]

Dudhia, J., 1989: Numerical study of convection observed during the Winter Monsoon Experiment using a mesoscale two-dimensional model. *J. Atmos. Sci.,* **46,** 3077–3107.

Dupont, S., T. L. Otte, and K. S. Ching, 2004: Simulation of meteorological fields within and above urban and rural canopies with a mesoscale model. *Bound.-Layer Meteor.,* **113,** 111–158.

Ek, M. B., K. E. Mitchell, Y. Lin, E. Rogers, P. Grunmann, V. Koren, G. Gayno, and J. D. Tarpley, 2003: Implementation of Noah land surface model advances in the National Centers for Environmental Prediction operational mesoscale Eta Model. *J. Geophys. Res.,* **108,** 8851, doi:10.1029/2002JD003296.

Fan, S., and Coauthors, 2008: Application of WRF 3D-Var to a high resolution model over Beijing area (in Chinese with English abstract). *Plateau Meteor.,* **27,** 1181–1188.

Grell, G. A., and D. Devenyi, 2002: A generalized approach to parameterizing convection combining ensemble and data assimilation techniques. *Geophys. Res. Lett.,* **29,** 1693, doi:10.1029/2002GL015311.

Guo, X., D. Fu, and J. Wang, 2006: Mesoscale convective precipitation system modified by urbanization in Beijing city. *Atmos. Res.,* **82,** 112–126.

Hjemfelt, M. R., 1982: Numerical simulation of the effects of St. Louis on mesoscale boundary-layer airflow and vertical motion: Simulations of urban vs. non-urban effects. *J. Appl. Meteor.,* **21,** 1239–1257.

Huff, F. A., and S. A. Changnon Jr., 1972: Climatological assessment of urban effects on precipitation at St. Louis. *J. Appl. Meteor.,* **11,** 823–842.

——, and ——, 1973: Precipitation modification by major urban areas. *Bull. Amer. Meteor. Soc.,* **54,** 1220–1232.

Janjic, Z. I., 1990: The step-mountain coordinate: Physical package. *Mon. Wea. Rev.,* **118,** 1429–1443.

——, 1994: The step-mountain eta coordinate model: Further developments of the convection, viscous sublayer, and turbulence closure schemes. *Mon. Wea. Rev.,* **122,** 927–945.

Jaurequi, E., and E. Romales, 1996: Urban effects on convective precipitation in Mexico City. *Atmos. Environ.,* **30,** 3383–3389.

Kusaka, H., H. Kondo, Y. Kikegawa, and F. Kimura, 2001: A simple single-layer urban canopy model for atmospheric models: Comparison with multi-layer and slab models. *Bound.-Layer Meteor.,* **101,** 329–358.

Landsberg, H. E., 1970: Man-made climate changes. *Science,* **170,** 1265–1274.

Lean, H. W., and Coauthors, 2008: Characteristics of high-resolution versions of the Met Office Unified Model for forecasting convection over the United Kingdom. *Mon. Wea. Rev.,* **136,** 3408–3424.

LeMone, M. A., F. Chen, M. Tewari, J. Dudhia, B. Geerts, Q. Miao, R. L. Coulter, and R. L. Grossman, 2010: Simulating the IHOP_2002 fair-weather CBL with the WRF-ARW–Noah modeling system. Part II: Structures from a few kilometers to 100 km across. *Mon. Wea. Rev.,* **138,** 745–764.

Li, Q., C. Zhang, and S. Miao, 2005: The distribution characteristics of rainfall and the effect of land use in Beijing area (in Chinese with English abstract). *J. Desert Res.,* **25** (Suppl.), 60–65.

Lin, C.-Y., and Coauthors, 2008: Urban heat island effect and its impact on boundary layer development and land–sea circulation over northern Taiwan. *Atmos. Environ.,* **42,** 5635–5649.

Liu, Y., F. Chen, T. Warner, and J. Basara, 2006: Verification of a mesoscale data-assimilation and forecasting system for the Oklahoma City area during the Joint Urban 2003 field project. *J. Appl. Meteor. Climatol.,* **45,** 912–929.

Martilli, A., A. Clappier, and M. W. Rotach, 2002: An urban surface exchange parameterisation for mesoscale models. *Bound.-Layer Meteor.,* **104,** 261–304.

Masson, V., 2000: A physically-based scheme for the urban energy budget in atmospheric models. *Bound.-Layer Meteor.,* **94,** 357–397.

——, 2006: Urban surface modeling and the meso-scale impact of cities. *Theor. Appl. Climatol.,* **84,** 35–45.

Miao, S., and F. Chen, 2008: Formation of horizontal convective rolls in urban areas. *Atmos. Res.,* **89,** 298–304.

——, ——, M. A. LeMone, M. Tewari, Q. Li, and Y. Wang, 2009a: An observational and modeling study of characteristics of urban heat island and boundary layer structures in Beijing. *J. Appl. Meteor. Climatol.,* **48,** 484–501.

——, P. Li, and X. Wang, 2009b: Building morphological characteristics and their effect on the wind in Beijing. *Adv. Atmos. Sci.,* **26,** 1115–1124.

Pielke, R. A., and R. P. Pearce, 1994: *Mesoscale Modeling of the Atmosphere. Meteor. Monogr.,* No. 47, Amer. Meteor. Soc., 167 pp.

Rosenfeld, D., J. Dai, X. Yu, Z. Yao, X. Xu, X. Yang, and C. Du, 2007: Inverse relations between amounts of air pollution and orographic precipitation. *Science,* **315,** 1396–1398.

——, U. Lohmann, G. B. Raga, C. D. O'Dowd, M. Kulmala, S. Fuzzi, A. Reissell, and M. O. Andreae, 2008: Flood or drought: How do aerosols affect precipitation? *Science,* **321,** 1309–1313.

Rotunno, R., Y. Chen, W. Wang, C. Davis, J. Dudhia, and G. J. Holland, 2009: Large-eddy simulation of an idealized tropical cyclone. *Bull. Amer. Meteor. Soc.,* **90,** 1783–1788.

Rozoff, C. M., W. R. Cotton, and J. O. Adegoke, 2003: Simulation of St. Louis, Missouri, land use impacts on thunderstorms. *J. Appl. Meteor.,* **42,** 716–738.

Sailor, D. J., 2011: A review of methods for estimating anthropogenic heat and moisture emissions in the urban environment. *Int. J. Climatol.,* **31,** 189–199.

Schlünzen, K. H., and J. J. Katzfey, 2003: Relevance of sub-grid-scale land-use effects for mesoscale models. *Tellus,* **55A,** 232–246.

Shepherd, J. M., H. Pierce, and A. J. Negri, 2002: Rainfall modification by major urban areas: Observations from spaceborne rain radar on the TRMM satellite. *J. Appl. Meteor.,* **41,** 689–701.

Skamarock, W. C., J. B. Klemp, J. Dudhia, D. O. Gill, D. M. Barker, W. Wang, and J. G. Powers, 2005: A description of the Advanced Research WRF version 2. NCAR Tech. Note TN-468+STR, 88 pp.

Souch, C., and S. Grimmond, 2006: Applied climatology: Urban climate. *Prog. Phys. Geogr.,* **30,** 270–279.

van den Heever, S. C., and W. R. Cotton, 2007: Urban aerosol impacts on downwind convective storms. *J. Appl. Meteor. Climatol.,* **46,** 828–850.

Wang, X., F. Chen, Z. Wu, M. Zhang, M. Tewari, A. Guenther, and C. Wiedinmyer, 2009: Impacts of weather conditions modified by urban expansion on surface ozone: Comparison between the Pearl River Delta and Yangtze River Delta regions. *Adv. Atmos. Sci.,* **26,** 962–972.

Zhang, C. L., F. Chen, S. G. Miao, Q. C. Li, X. A. Xia, and C. Y. Xuan, 2009: Impacts of urban expansion and future green planting on summer precipitation in the Beijing metropolitan area. *J. Geophys. Res.,* **114,** D02116, doi:10.1029/2008JD010328.

Zhao, W., and J. Wang, 2008: Comparison and analysis on two successive torrential rain events over Beijing in summer of 2006 (in Chinese with English abstract). *Meteor. Mon.,* **34,** 3–14.